Landmarks in Earth Reinforcement, Ochiai et al. (eds),
© 2001 Swets & Zeitlinger, ISBN 90 2651 863 3

Bearing capacity considering stiffness of reinforcement material

K. Arai & M. Kamon
Fukui University, Fukui, Japan

S. Nomura & Y. Yokota
Maeda Kosen Co. Ltd., Fukui, Japan

ABSTRACT: This paper proposes a practical procedure for estimating the bearing capacity of strip footing on reinforced ground. The procedure aims to fill a gap existing between classical FEM and conventional limit equilibrium analysis, by creating a definite collapse mechanism analogous to a slip surface. Based on Mohr-Coulomb yield criterion, a simple non-associated flow rule, a smeared shear band approach, and on an improved initial stress method, the procedure provides an explicit collapse mechanism represented by stress yield condition. Since the collapse mechanism is supported by a displacement field and a stress field, the procedure enables to perform stability analysis taking the stiffness and deformation into consideration.

1 INTRODUCTION

Conventional stability analysis based on limit equilibrium method tends to become uncertain, when a soil stratum consists of multiple layers, or when it includes other materials having quite different stiffness like earth reinforcement materials. This is because limit equilibrium method evaluates the material properties only by its final strength. The method represents kinematical conditions only by using the mechanically reasonable shape of a slip surface, and does not explicitly allow to consider the stiffness and deformation of materials, which seem to play an important role for evaluating earth reinforcement methods, and which may affect the global collapse mode. To compensate for these defects, a lot of trials have been made by applying other analytical methods, for instance, FEM and limit analysis. In order to utilize these analytical methods in the practical design, the methods are expected to provide an explicit collapse mode as well as a slip surface used in stability analysis, because the results by these methods should be related closely to the conventional solutions. Classical FEM does not necessarily provide a reasonable collapse mechanism. Subjected to Mohr-Coulomb material, the limit analysis method has not completely overcome the difficulty that the limit theorems cannot be proven without the normality rule in plasticity, and that the normality rule may not hold for the material. In spite of many researches in recent years, the accurate description of localization phenomenon in soils is still open to question. For instance, the bifurcation analysis which tries to simulate actual localized deformation, seems to give a promising view, while the analysis may not give reasonable solutions for complicated boundary value problems like bearing capacity. Still now the stability analysis considering both reasonable collapse mode and material stiffness, remains a thorny subject for practical design work. Using a modification of the smeared shear band approach (Pietruszczak et al., 1981) which is based on estimating average mechanical properties of elastic solid and shear band, and using a new calculation scheme for nonlinear FE analysis, this paper aims to develop a practical procedure for estimating the bearing capacity, which enables to create a reasonable collapse mode supported by a displacement field. This paper treats only a centrally and vertically loaded strip footing on flat subsoil under the plane strain condition.

2 CONSTITUTIVE RELATIONSHIP

2.1 *Yield criterion*

To relate the proposed procedure to conventional stability analysis, Mohr-Coulomb and Coulomb yield criteria are employed respectively to plane strain soil mass and friction interface between structure and soil. For the friction interface we employ the thin layer finite element as shown in Fig. 1 (Desai et al., 1984).

Mohr-Coulomb:

$$F_M=\{(\sigma_x-\sigma_y)^2+4\tau_{xy}^2\}^{1/2}-$$

$$\{(\sigma_x+\sigma_y)\sin\phi+2c\cos\phi\}=0 \quad (1)$$

Coulomb:

$$F_C=|\tau_{st}|-c-\sigma_t\tan\phi=0 \quad (2)$$

where σ_x, σ_y and τ_{xy}: stress components, σ_t and τ_{st}: normal and shear stresses in friction interface (see Fig. 1), and c and φ: cohesion and friction angle. Both quadrilateral plane strain and thin layer finite elements are built up from four constant strain triangles, and a set of stresses is regarded constant within each element.

2.2 *Coulomb interface*

Both for Mohr-Coulomb and Coulomb materials, a linear elastic response is assumed before yielding. Fig. 2 schematically illustrates the relationship between stress vector $\{\sigma\}$ and strain vector $\{\varepsilon\}$. When applying further footing pressure after a stress state has reached the yield surface, the stress state will move along the yield surface as seen in Fig. 2. This is because normal stress σ_t becomes larger with the increase in footing pressure, and because yielding shear stress increases with normal stress for frictional material. Point B in Fig. 2 corresponds to a plastic equilibrium state at an arbitrary position within a yield region. At the elasto-plastic state from point A to B shown in Fig. 2, we employ the simplest non-associated flow rule or plastic potential Qc defined by Fig. 3 (Mroz, 1980)

$$Qc = |\tau_{st}| - g - \sigma_t \tan\nu \qquad (3)$$

where ν: dilatancy angle (see Fig. 3) and g: a hypothetical parameter which is not cited actually, because Qc is used only by its differential form. For the thin layer element shown, Eqs. (2) and (3) give the elasto-plastic stress-strain relationship as (Zienkiewicz et al. 1969)

$$\{\delta\sigma\}=[D_{st}^{ep}]\{\delta\varepsilon^{ep}\} \qquad (4)$$

$$\{\delta\sigma\}=\{\delta\sigma_s, \delta\sigma_t, \delta\tau_{st}\}^T$$
$$\{\delta\varepsilon^{ep}\}=\{\delta\varepsilon_s^{ep}, \delta\varepsilon_t^{ep}, \delta\gamma_{st}^{ep}\}^T$$
$$[D_{st}^{ep}] =[D]-[D]\{\partial Fc/\partial\{\sigma\}\}$$
$$\times\{\partial Qc/\partial\{\sigma\}\}^T[D] / \{\partial Fc/\partial\{\sigma\}\}^T$$
$$\times[D]\{\partial Qc/\partial\{\sigma\}\}$$

where $\{\delta\sigma\}$ and $\{\delta\varepsilon^{ep}\}$: stress and elasto-plastic strain increments (Fig. 2), $[D_{st}^{ep}]$: elasto-plastic stress-strain matrix in local coordinate s-t in Fig. 1, $[D]$: elastic matrix, E: Young's modulus, μ: Poisson's ratio, and G: rigidity modulus.

2.3 *Mohr-Coulomb material*

When shearing a finite size of soil element, it is well known that we often observe a shear band or slip surface as shown in Fig. 4 (a). Despite many theoretical and experimental studies concerning the mechanism of shear band formation, we have not reached a final agreement with regard to inclination angle of shear band α defined in Fig. 4 (a) (e.g. Vardoulakis et al., 1980). Since our main concern is to

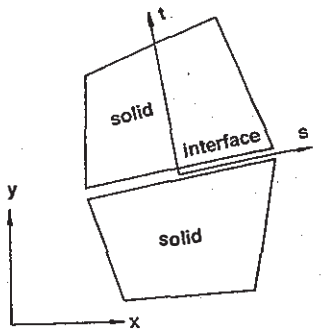

Figure 1. Interface element.

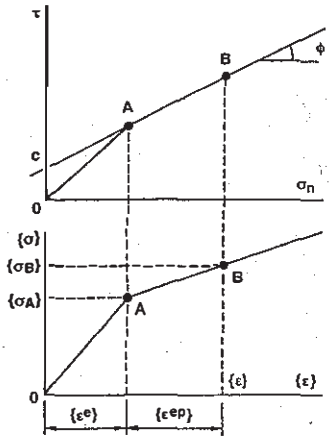

Figure 2. Stress-strain relationship (Coulomb material).

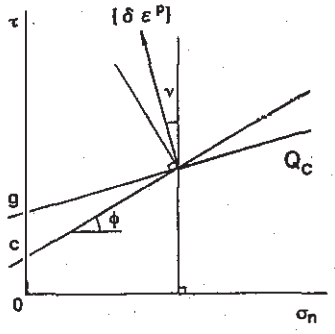

Figure 3. Non-associated flow rule (Coulomb material).

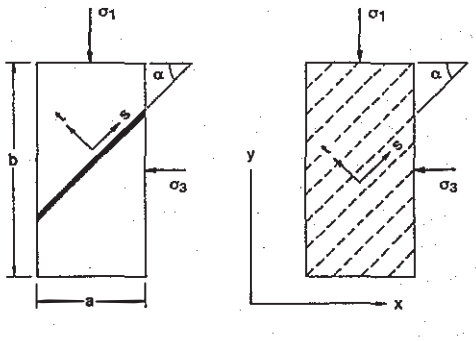

Figure 4. Shear band formation.

get a practical design procedure, we employ the most fundamental expression as

$$\alpha = \pi/4 + \phi/2 \quad (5)$$

Without introducing a separate interface element corresponding to a shear band, Pietruszczak et al. (1981) proposed the smeared shear band approach which evaluated the average stress-strain response of solid and shear band. This approach assumes elastic response of solid and purely plastic response of shear band. Herein we assume elastic response of solid and elasto-plastic response of shear band, because this postulate yields a convenient constitutive behavior as described later. According to the procedure by Pietruszczak et al. (1981), the average stress-strain matrix is given as follows. Assume that a plane strain solid element reaches a yield state, and that a shear band has been created as shown in Fig. 4 (a). Regarding the shear band as a thin layer element shown in Fig. 1, strains in shear band are given in local coordinate s-t as (Eq. 4)

$$\{\delta\varepsilon^{ep}\} = [D_{st}^{ep}]^{-1}\{\delta\sigma\} \quad (6)$$

Assuming elastic response except in shear band, strains in solid region are

$$\{\delta\varepsilon^{e}\} = [D]^{-1}\{\delta\sigma\} \quad (7)$$

Superposing these two strains by Pietruszczak et al. (1981), average stress-strain matrix of the whole element $[D_{st}^{av}]$ and that in global coordinate x-y $[D_{xy}^{av}]$ are

$$[D_{st}^{av}] = \{[D_{st}^{ep}]^{-1} t / \sqrt{A}\ \cos\beta + [D]^{-1}(1 - t/\sqrt{A} \times \cos\beta)\}^{-1} \quad (8)$$

$$[D_{xy}^{av}] = [T]^{T}[D_{st}^{av}]\,[T] \quad (9)$$

where t: thickness of shear band, and $[T]$: coordinate transformation matrix. Both $[D_{st}^{av}]$ and $[D_{xy}^{av}]$ include no current stress components. The average matrix calculated above becomes close to the stress-strain matrix for the stratified or cross anisotropic material which is built up from the Coulomb material represented by a thin layer element as illustrated in Fig. 4 (b).

2.4 *Direction of shear band*

Generally a set of two shear bands or slip surfaces A-A' and B-B' is possible for a finite soil element according to the principal stress state as shown in Fig. 5. In practical problems we must select one of these two shear bands. Since our object is to get a practical method for stability analysis, we make efficient use of the conventional collapse mode as illustrated in Fig. 6. Many experimental researches have observed actually the active wedge developing in model test. A lot of bifurcation analyses also have obtained the active wedge, while the analyses have not got the complete collapse mode as illustrated in Fig. 6. Based on these results, we assume the active

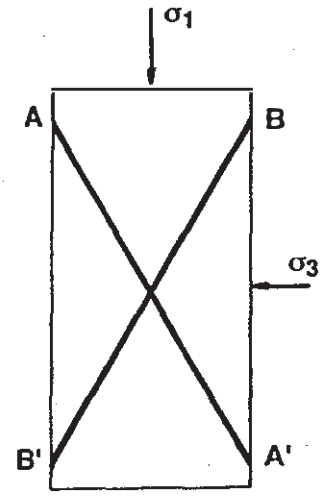

Figure 5. A set of two slip surfaces.

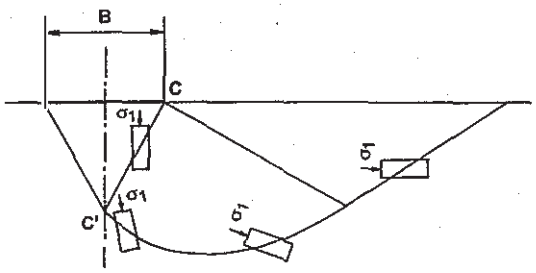

Figure 6. Isolation of slip surface.

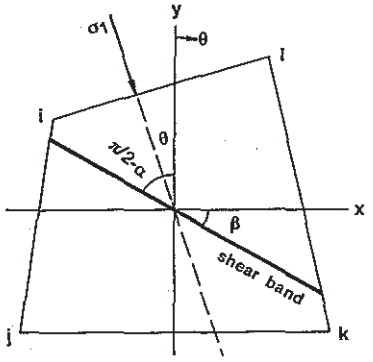

Figure 7. Direction of slip surface in a element.

wedge below strip footing base, which is represented by a series of interface elements in Fig. 9 shown later. Thus we employ the right-hand side shear band B-B' defined in Fig. 5 within the active wedge in Fig. 9, and assume the left-hand side shear band A-A' in Fig. 5 outside of the active wedge as seen in Fig. 6. Referring to Fig. 7, the direction of A-A' or B-B' line in Fig. 6 is given as

$$\beta = -\alpha - \theta \quad : \text{A-A' line}$$
$$= \alpha - \theta \quad : \text{B-B' line} \quad (10)$$

where β: inclination angle of shear band, and θ: angle of the major principal stress from vertical axis

(Fig. 7). Note that compressive stress is positive here and that shear stress τ_{st} is negative along A-A' line in Fig. 6 and positive along B-B' line.

3 NUMERICAL PROCEDURE

3.1 *Fundamental aspect*

Fig. 8 defines actual stress of initial state $\{\sigma_I\}$, yield stress $\{\sigma_A\}$, actual stress of plastic equilibrium state $\{\sigma_B\}$, elastic stress $\{\sigma_E\}$, virtual initial stress $\{\sigma_0\}$, total strain $\{\varepsilon\}$, elastic strain $\{\varepsilon^e\}$, and elasto-plastic strain $\{\varepsilon^{ep}\}$. 1) For the convenience of solving bearing capacity problems, we apply footing pressure by many loading stages subdivided. In the application of initial stress method, we use the same stiffness matrix throughout all the loading stages, because we assume linear response of subsoil both before and after yielding. 2) Yield stress $\{\sigma_A\}$ is isolated by Zienkiewicz et al. (1969) 3) To determine the direction of shear band as shown in Fig. 7, it is necessary to find direction of the major principal stress θ. We decide θ by using yield stress $\{\sigma_A\}$, and use it throughout the succeeding loading stages.

3.2 *Improved initial stress method*

The original initial stress method often provides unstable results for our problem. The incremental procedure which treats the nonlinearity as piecewise linear, does not create the collapse mode as illustrated in Fig. 6. These difficulties are avoided by introducing an iteration scheme based on the conjugate gradient method (CGM, Flecher et al. 1964) instead of the original initial stress method. CGM is often used for solving simultaneous linear equations with quite many unknowns, for the purpose of reducing computational effort. The constitutive model employed here, which is a linear equation also at elasto-plastic state, enables to apply effectively CGM. Since $\{\sigma_0\} = \{\sigma_E\} - \{\sigma_B\}$, the basic equation is given as

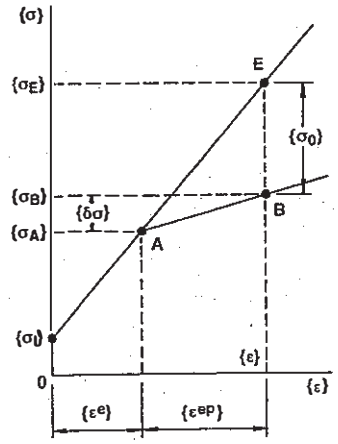

Figure 8. Initial stress method.

$$\{r\}_i=\{\sigma_0\}_i-\{\sigma_E\}_i+\{\sigma_B\}_i$$
$$= \{\sigma_0\}_i- ([D]_i-[D_{xy}{}^{av}]_i)[B]_i\{[K]^{-1}(\{\delta f\}$$
$$+\Sigma_j[B]_j{}^T\{\sigma_0\}_jA_j)\}_i=0 \quad (11)$$

where $\{r\}_i$: residual, $[B]_i$: matrix for calculating strain components from nodal displacements, $[K]$: global stiffness matrix, $\{\delta f\}$: load increment vector, A_i: area of the element, and suffixes i and j denote element number.

The iteration procedure by CGM is as follows. 1) Set the trial values of $\{\sigma_0\}$. 2) Calculate gradient $\{g\}^n$ given by Eq. (12), where n designates an iteration number. 3) $\{d\}^n=-\{g\}^n+\{d\}^{n-1}\cdot\{g\}^n{}^T\{g\}^n/\{g\}^{n-1}{}^T\{g\}^{n-1}$. 4) $\{\sigma_0\}^{n+1}=\{\sigma_0\}^n+\lambda^n\{d\}^n$. 5) Repeat 1) to 4) until $\{r\}_i$ becomes sufficiently small. $\{g\}^n$ and λ^n are calculated analytically. Conclusively the numerical steps during a typical load increment are summarized as follows. 1) Performing an elastic analysis by using actual load increment $\{\delta f\}$, calculate $\{\sigma_E\}$ and $\{\varepsilon\}$ in Fig. 8. 2) Find the yield finite elements in which $\{\sigma_E\}$ violates the yield criterion. 3) For the yield elements, calculate yield stress $\{\sigma_A\}$ both from $\{\sigma_E\}$ and the preceding stress state. 4) Concerning $\{\sigma_A\}$, calculate direction of the major principal stress θ, and find shear band inclination angle β by Eq. (10) (Fig. 8). 5) Calculate $[D_{xy}{}^{av}]$ by Eq. (9). 6) Determine $\{\sigma_0\}$ by CGM. 7) Again, find the yield finite elements by performing an elastic analysis by use of both $\{\delta f\}$ and $\{\sigma_0\}$ determined at 6). When finding new yield elements, determine $\{\sigma_0\}$ by CGM subjected to the total yield elements including the new yield elements. Repeat this procedure until no new yield elements are found. 8) Based on the final results at 7), calculate necessary state variables $\{\sigma_B\}$, settlements, and so on.

4 CASE STUDIES

We discuss the effect of earth reinforcement, concerning the bearing capacity of a rigid strip footing on a homogeneous and ponderable c-ϕ soil stratum. FE meshing and material parameters are given in Fig. 9, in which γ: unit weight, T: thickness of footing and A: area of cross section of truss material. As described before, the active wedge below footing base is assumed by a series of interface elements, so as to isolate the direction of shear band (Fig. 5). Angle α in Fig. 9 is given by Eq. (5), regarding the vertical footing pressure as the major principal stress. Actual initial stress vector $\{\sigma_I\}$ is given as: vertical stress σ_{yI}=overburden pressure, horizontal stress $\sigma_{xI}=K_0\sigma_{yI}$, and $\tau_{xyI}=0$, where $K_0=1-\sin\phi$. For convenience, we introduce 'footing pressure ratio R' defined as

$$R = q / q_u \quad (12)$$

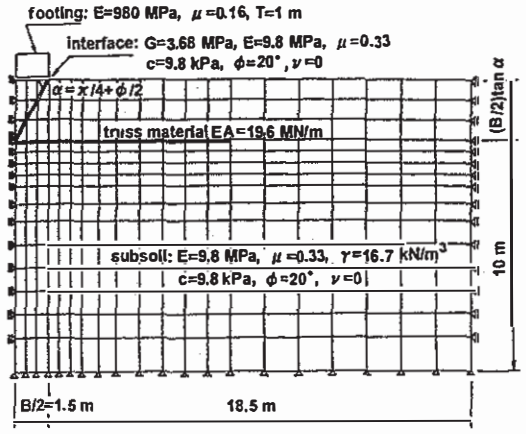

Figure 9. FE meshing.

where q: current footing pressure applied, and q_u: ultimate bearing capacity given by Terzaghi. R is increased step by step at each loading stage subdivided. Fig. 10 shows the relationship between R and footing settlement calculated by the proposed procedure. When ϕ exceeds 25°, the iteration by CGM does not converge at a certain loading step. This suggests that we cannot find a plastic equilibrium state B shown in Fig. 2 for larger R, which is considered as the bearing capacity. When CGM converges at every loading stage, we regard the bearing capacity as the footing pressure at which settlement increases remarkably, or as the pressure at which R-settlement curve merges into the approximate straight line observed after R has exceeded the critical pressure, as shown in Fig. 10. This is because the straight line means the plastic flow of foundation subsoil. The bearing capacity in terms of R is called 'critical footing pressure ratio R_{cr}'. As shown in Fig. 10, this earth reinforcement method increases R_{cr} from 1 (no reinforcement) to 1.3. Fig. 11 compares the yield region respectively for reinforced ground with natural ground, in which the bold solid line in each finite element represents the direction of shear band as shown in Fig. 4 (a), and that the element has yielded. Fig. 11 (a) seems to produce a collapse mode analogous to Prandtl mechanism given for imponderable subsoil. More complete collapse mode is observed for larger R. The collapse mode in Fig. 11 is supported by the displacement field shown in Fig. 12 and stress field shown in Fig. 13. That is, the collapse mode is created by considering the weight of subsoil, stiffness of footing and subsoil, friction between footing and subsoil, and stress concentration at the edge of rigid footing, most of which are ignored in Prandtl and Terzaghi approaches. The yield region in Fig. 11 tends to distribute deeply below footing. Despite the lateral plastic flow as illustrated in Fig. 11, the vertical pressure must reach lower subsoil due to the vertical equilibrium condition, and the pressure makes lower subsoil yield. Although conventional stability analysis provides little information about yield state except on the location of slip surface, there is the possibility that the region lower than the slip surface may yield. In Fig. 12 we observe little deformation of lower subsoil. The proposed procedure represents a collapse mode by yield condition of stresses, which is the same as conventional stability analysis and different from most application of conventional FEM using strain distribution. The conventional design scheme based on stability analysis, uses the collapse mechanism assumed without reinforcement, and evaluates the reinforcement only by its final strength. The scheme neglects the stiffness of reinforcement material which may restrict the deformation of subsoil and which may largely contribute to the improvement of bearing capacity. This example proves the possibility of applying the proposed procedure to the stabil-

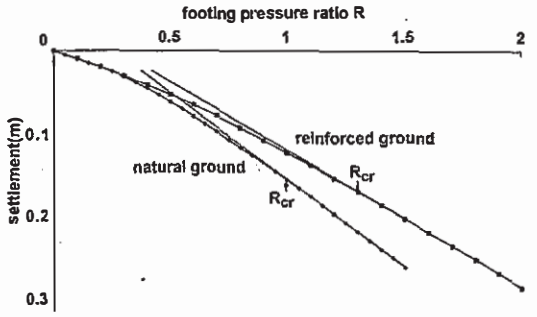

Figure 10. R-settlement curves.

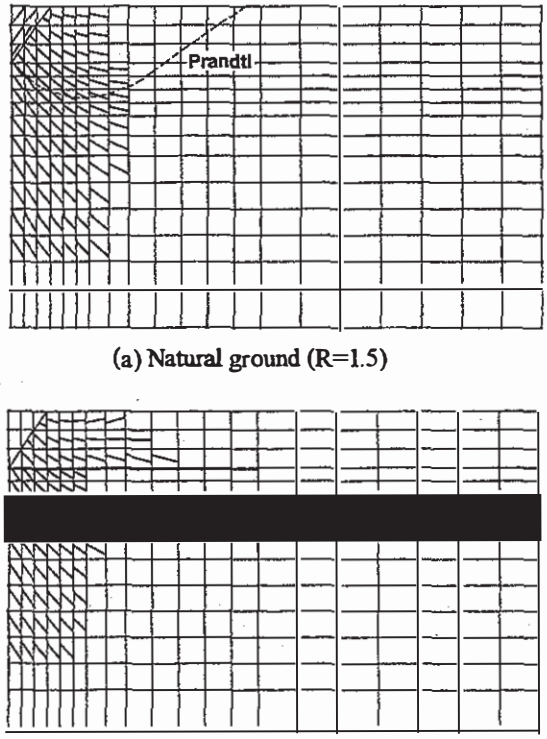

(a) Natural ground (R=1.5)

(b) Reinforced ground (R=1.5)

Figure 11. Yield region.

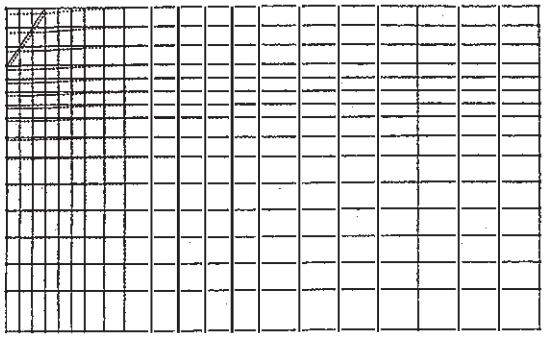

Figure 12. Displacement field (reinforced, R=1.5).

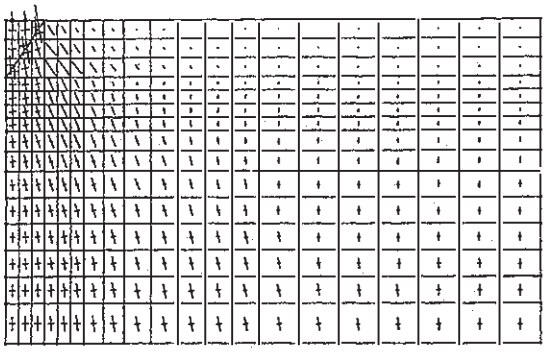

Figure 13. Principal stresses (reinforced, R=I.5).

ity analysis of earth reinforcement, which takes the stiffness and displacement of material into consideration.

5 CONCLUSIONS

This paper proposed a numerical procedure for analyzing the bearing capacity of strip footing. The procedure aims to fill a gap existing between conventional stability analysis and classical FEM. The procedure employs Mohr-Coulomb and Coulomb yield criteria respectively for soil mass and friction interface between soil and structure. By assuming a linear elastic response before yielding and a simple non-associated flow rule after yielding, and by employing a modified smeared shear band approach and an improved initial stress method, the procedure provides an explicit collapse mechanism like a slip surface. At the collapse mode, a stress yield criterion is satisfied as well as along a slip surface supposed in conventional stability analysis. Case studies show that the proposed procedure provides a solution close to the conventional solution, and show the possibility that the procedure gives a reasonable estimate of bearing capacity on reinforced ground.

REFERENCES

Desai, C. S., Zaman, M. M., Lightner, J. G. & Siriwardane, H. J. 1984. Thin-layer element for interfaces and joints. *Int. J. Numer. Anal. Methods Geomech.* 8: 19-43.

Flecher, R. & Reeves, C. M. 1964. Function minimization by conjugate gradient. *Computer J.* 7: 149-154

Mroz, Z. 1980. Deformation and flow of granular materials. *Mechanics of Solids* (the Rodney Hill 60th Anniversary Volume) Pergamon Press, Oxford. 119-132.

Ortiz, M., Leroy, Y. & Needleman, A. 1987. A finite element method for localized failure analysis. *Computer Methods Appl. Mech. Eng.* 61: 189 - 214.

Pietruszczak, S. & Mroz, Z. 1981. Finite element analysis of deformation of strain-softening materials. *Int. J. Num. Methods Eng.* 17:327-334

Vardoulakis, I. 1980. Shear band inclination and shear modulus of sand in biaxial tests. *Int. J. Num. Ana. Methods Geomech.* 4:103-119.

Zienkiewicz, O. C., Valliappan, S. & King, I. P. 1969. Elastoplastic solutions of engineering problems 'initial stress', finite element approach. *Int. J. Numer. Methods Eng.* 1: 75-100.